THE PHOTO-OXIDATION OF i-C_3H_7CHO VAPOUR

JAYANT DESAI, JULIAN HEICKLEN, ABRAHA BAHTA and R. SIMONAITIS

Department of Chemistry and Communications and Space Sciences Laboratory, The Pennsylvania State University, University Park, PA 16802 (U.S.A.)

(Received November 21, 1985; in revised form February 13, 1986)

Summary

The steady state photolysis of *iso*-butyraldehyde (i-C_3H_7CHO) was studied in the presence of O_2 at 263 and 294 K at several incident wavelengths. The quantum yields of CO and C_3H_8 were measured. From them the primary quantum yield $\Phi(C_3H_8)$ of the molecular process to produce CO + C_3H_8 and the primary quantum yield Φ(rad) of the free-radical process to produce i-C_3H_7 + HCO were deduced. Likewise the flash photolysis of i-C_3H_7CHO was studied in the presence of air at 298 K. The transient absorption of RO_2 radicals was monitored, and relative quantum yields were obtained with 284.0, 302.5, 311.7, 325.0 and 330.5 nm incident radiation. The quantum yields were not pressure quenched, except for very slightly at 330.5 nm. They followed the same trends with incident wavelength as seen in the steady state photolysis.

The mechanism describing the primary process is

$$A + h\nu \longrightarrow {}^1A_n \quad (1)$$

$${}^1A_n \longrightarrow CO + RH \quad (2a)$$

$$\longrightarrow A_n \quad (2b)$$

$$\longrightarrow {}^3A_n \quad (2c)$$

$${}^3A_n \longrightarrow HCO + R \quad (5)$$

$${}^3A_n + M \longrightarrow {}^3A_0 + M \quad (6)$$

$${}^3A_n + A \longrightarrow A_n + A \quad (8a)$$

$$A_n \longrightarrow CO + RH \quad (3)$$

$$A_n + M \longrightarrow A + M \quad (4)$$

$$A_n + A \longrightarrow A + \text{removal of } A_n \quad (7)$$

where R represents i-C_3H_7, A represents the aldehyde, the superscripts 1 and 3 represent excited singlet and triplet states respectively, the subscripts n

0047-2670/86/$3.50

and 0 represent excited and ground vibrational levels respectively and M represents O_2 and N_2. $k_{2a}/k_2 = 0.43$ and $k_{2a}/k_2 = 0.31$ at 253.7 nm and 280.3 nm respectively and $k_{2a}/k_2 = 0$ at 302.2 nm and longer wavelengths. The quenching of ^3A_n by O_2 or N_2 is quite inefficient, the half-pressure for quenching increasing with temperature and incident energy. Under all conditions studied it is 1200 Torr or greater. However, quenching of ^3A_n by i-C_3H_7CHO is quite efficient with $k_5/k_{8a} = 32.1 \pm 10.0$ Torr at 312.8 nm and 294 K. The quenching of A_n is insensitive to variations in temperature or incident energy. An approximate value for k_3/k_4 was estimated to be about 108 Torr. From the mechanism, radical quantum yields could be estimated at atmospheric pressure at several wavelengths. These lead to atmospheric photodissociation coefficients for radical formation at 298 K of 7.6×10^{-5} s^{-1} and 5.9×10^{-5} s^{-1} for solar zenith angles of 30° and 58° respectively.

1. Introduction

The photodissociation of aldehydes is important in the production of photochemical smog. The radical products are responsible for driving the chemical cycles which convert NO to NO_2. Therefore a number of studies on the simple aliphatic aldehydes have been undertaken in recent years. These include studies on CH_2O [1 - 23], CH_3CHO [1, 24 - 42] and C_2H_5CHO [43 - 50].

From these studies, a general picture of the primary process has emerged. The mechanism is believed to be

$$A + h\nu \longrightarrow {}^1A_n \quad (1)$$

$${}^1A_n \longrightarrow CO + RH \quad (2a)$$

$$\longrightarrow A_n \quad (2b)$$

$$\longrightarrow {}^3A_n \quad (2c)$$

$$\longrightarrow A + h\nu_f \quad (2d)$$

$$A_n \longrightarrow CO + RH \quad (3)$$

$$A_n + M \longrightarrow A + M \quad (4)$$

$${}^3A_n \longrightarrow HCO + R \quad (5)$$

$${}^3A_n + M \longrightarrow {}^3A_0 + M \quad (6)$$

where A represents the aldehyde, the superscripts 1 and 3 represent excited singlet and triplet states respectively, and the subscripts n and 0 represent excited and ground vibrational levels respectively.

The photolysis of *iso*-butyraldehyde (i-C_3H_7CHO) has been examined in a few studies. The early studies [51, 52] were devoted to determining the products and their quantum yields. The major products were found to be CO, C_3H_8 and radical products expected from i-C_3H_7 radicals, together with a small amount of H_2 ($\Phi = 0.03$ [52]).

Borkowski and Ausloos [45] measured the relative fluorescence yields at 308, 342 and 392 K with 313.0 nm incident radiation and at 308 K with 334.0 nm incident radiation. With 313.0 nm radiation, the fluorescence yield decreased by about 30% at 308 K, remained unaffected at 342 K and decreased by 15% at 392 K as the i-C_3H_7CHO concentration was increased from 0.16×10^{-3} to 5.73×10^{-3} M. With 334.0 nm radiation at 308 K, the fluorescence yield was unchanged as the concentration was raised. For all practical purposes, we can assume the fluorescence yields to be independent of pressure in conformance with expectations from the mechanism presented above.

Borkowski and Ausloos [45] also measured the phosphorescence of biacetyl induced by ground vibrational levels of triplet i-C_3H_7CHO. This yield increased with i-C_3H_7CHO pressure (334.0 nm radiation; 306 K) in conformance with the above mechanism. The half-quenching pressure was about 40 Torr.

Encina *et al.* [53] measured the lifetime and self-quenching of the excited singlet state of i-C_3H_7CHO in hexane solution. They found the zero-pressure lifetime to be 1.0 ns and the self-quenching rate coefficient to be 2.0×10^9 M^{-1} s^{-1}. Combination of these two values leads to a calculated half-quenching pressure of 4800 Torr.

We have undertaken to obtain the product quantum yields as a function of pressure, wavelength and temperature for i-C_3H_7CHO. Those results are reported here.

2. Experimental details

2.1. Steady state photolysis

The steady state photolysis was performed as described by Heicklen *et al.* [54]. The total pressure was brought to the desired value by adding dry O_2 and, in some cases, N_2.

The experiments were performed at 253.7, 280.3, 302.2, 312.8, 326.1 and 334.1 nm. A Hanovia medium pressure lamp (type SH) together with a Hanovia lamp stabilizer (type 30620) was used for the 280.3, 302.2, 312.8 and 334.1 nm lines. The 312.8 nm line and the 334.1 nm line were isolated by using Corion SM 3130-2 and SM-3340-2 interference filters respectively. The bandwidth full width at half-maximum (FWHM) of these filters is approximately 8 nm. The 280.3 nm line was isolated by using a P/N 35-2849-99 interference filter of diameter 1 in from the Ealing Corporation. Its peak emission is at 279.2 nm and it has a bandwidth (FWHM) of 11.3 nm. In addition to the 280 nm line, the mercury line at 275.3 nm, which is con-

siderably weaker, was also passed. There is also a weak mercury line at 260.3 nm, but it contributes only 2% of the intensity of the 280.4 nm line. The 302.2 nm line was isolated using a Jarrell–Ash 0.25 meter Ebert monochromator (model 82-410). Both entrance and exit slits were 2 mm. The bandpass of the monochromator was 7.5 nm under these conditions. From the measured lamp intensities at 297 and 302 nm, it was determined that with the monochromator set at 302 nm, 14% of the light passing through the exit slit was from the 297 nm line.

For the experiments at 253.7 nm, a low pressure U-shaped mercury lamp (model 687-A45) from Conrad Hanovia was used. The 184.9 nm line was removed by absorption in the air before striking the cell.

The 326.1 nm line was isolated using a Philips cadmium resonance lamp (model Cd09A (93107E)) with a Corning 0-54 filter to remove the 228 nm line.

CO and C_3H_8 were the products of interest and were determined by gas chromatography with a thermal conductivity detector. CO was separated on a stainless steel column (5 ft × 1/4 in) packed with 5A molecular sieve. C_3H_8 was separated on a Teflon column (10 ft × 1/4 in) packed with Chromosorb 101 (diatomaceous earth). The molecular-sieve column was operated at room temperature with a helium flow rate of 60 ml min^{-1} whereas the Chromosorb 101 column was operated at 363 K with a helium flow rate of about 40 ml min^{-1}.

Azomethane was used as an actinometer at 312.8, 326.1 and 334.1 nm, and phosgene was used as an actinometer at 253.7 nm. Both actinometer procedures have been described by Heicklen *et al.* [54].

Since the quantum yield for CO production at low pressure (10 Torr each of O_2 and aldehyde) at 253.7, 312.8, 334.1 and 326.1 nm was found to be unity, actinometry at 280.3 and 302.2 nm was performed by photolysis at a low pressure of aldehyde and O_2, and Φ(CO) was assumed to be 1.0.

2.2. Flash photolysis

i-C_3H_7CHO (15 - 30 Torr) was photolyzed with a frequency-doubled dye laser at 284.0, 302.5, 311.7, 325.0 and 330.5 nm (uncertainty in wavelength measurement, ±0.3 nm) in the presence of 30 - 650 Torr of dry room air. The arrangement of the apparatus is essentially as described previously [41].

Actinometry for quantum yield determinations was done by photolyzing Cl_2–O_2–C_3H_8 mixtures (4 - 8 Torr Cl_2 in about 45 Torr O_2 which contained about 6.9 mol.% hydrocarbon). The absorption coefficients used for Cl_2 were those measured in our laboratory, while those used for *i*-C_3H_7CHO were taken from the literature [55]. Table 1 lists these absorption coefficients together with literature values. The photolysis of the Cl_2–O_2–C_3H_8 mixture generates both the *n*-$C_3H_7O_2$ and the *i*-$C_3H_7O_2$ radicals. The absorption cross sections of these radicals are not known. Thus absolute actinometry results cannot be obtained. Relative quantum yields were obtained by assuming the

TABLE 1

Absorption cross sections σ for i-C_3H_7CHO and Cl_2 at 298 K

λ (nm)	$10^{20}\sigma$ [a] (cm^2)	$10^{20}\sigma$ [b] (cm^2)
i-C_3H_7CHO		
284.0		5.70
302.5		5.43
311.7		3.76
325.0		1.84
330.5		0.89
Cl_2		
284.0	3.98	4.20
302.5	12.9	13.1
311.7	17.0	19.4
325.0	25.0	25.1
330.5	25.4	25.6

[a] This work.
[b] Literature values: for i-C_3H_7CHO, from Calvert and Pitts [55]; for Cl_2, from NASA [56].

same cross section for both radicals. Since in many cases these quantum yields significantly exceed 1.0, it is clear that this assumption is in error.

2.3. Materials

i-C_3H_7CHO (Aldrich, Gold Label, 99.7%) was purified by trap-to-trap distillation from 212 K to 142 K. Cl_2 (Matheson, research grade) was passed over KOH to remove HCl and was degassed at 77 K. The C_3H_8 (Matheson, ultrahigh purity) was used directly from the cylinder. Laboratory air was used after being dried by rapid passage through a trap at 77 K. The Matheson O_2, N_2, CO and C_3H_8 were extra dry, prepurified, chemically pure and chemically pure grade respectively. All gases were handled in a conventional glass vacuum line containing Teflon stopcocks and Viton O-rings. The Cl_2 pressure was measured using an H_2SO_4 manometer, the C_2H_5CHO pressure using a Wallace and Tiernan model FA-160 0-50 Torr absolute pressure indicator and the air using a calibrated NRC 820 Alphatron gauge.

3. Results

3.1. Steady state photolysis

i-C_3H_7CHO was photolyzed at several incident wavelengths in the presence of excess O_2 and in some cases O_2 and N_2. The products measured were CO and C_3H_8 since these products give a direct measure of two photodecomposition pathways:

$$i\text{-}C_3H_7CHO + h\nu \longrightarrow C_3H_8 + CO \quad \text{(i)}$$

$$\longrightarrow C_3H_7 + HCO \xrightarrow{O_2} HO_2 + CO \quad \text{(ii)}$$

The quantum yield $\Phi(C_3H_8)$ of C_3H_8 formation is a direct measure of the yield of the molecular process, whereas the quantum yield $\Phi(CO)$ of CO formation is a direct measure of the sum of the molecular and free-radical processes. Thus the quantum yield $\Phi(rad)$ of the radical process is given by $\Phi(CO) - \Phi(C_3H_8)$.

First, studies were done to determine the effect of the extent of conversion on the product quantum yields. The data for $\Phi(C_3H_8)$ are given in Table 2 for three incident wavelengths. It can be seen that the extent of conversion at 253.7 nm has only a small effect (7%) on $\Phi(C_3H_8)$, for conversions of up to 51 mTorr C_3H_8. Likewise at 280.0 nm a small fall-off (5%) in $\Phi(C_3H_8)$ occurs as the conversion increases from 6.5 to 28.5 mTorr C_3H_8. At 312.8 nm the effect is more dramatic and a considerable fall-off in $\Phi(C_3H_8)$

TABLE 2

Effect of conversion on C_3H_8 quantum yields in steady state photolysis

$[C_3H_8]$ (mTorr)	*Irradiation time* (min)	$\Phi(C_3H_8)$
λ = 253.7 nm, T = 294 K, $I_a = 1.70 \times 10^{-4}$ photons min^{-1} per $i\text{-}C_3H_7CHO$ molecule, $[i\text{-}C_3H_7CHO]$ = 10.1 ± 0.1 Torr, $[O_2]$ = 90 Torr		
10.7	10.0	0.63
20.8	20.0	0.61
31.7	32.0	0.58
40.0	40.0	0.58
50.9	50.0	0.59
λ = 280.3 nm, T = 294 K, $I_a = 6.6 \times 10^{-5}$ photons min^{-1} per $i\text{-}C_3H_7CHO$ molecule, $[i\text{-}C_3H_7CHO]$ = 10.0 ± 0.1 Torr, $[O_2]$ = 15 Torr		
6.5	15.0	0.65
12.8	30.0	0.64
16.6	40.0	0.63
24.9	60.0	0.62
28.5	70.0	0.62
λ = 312.8 nm, T = 294 K, $I_a = 4.5 \times 10^{-4}$ photons min^{-1} per $i\text{-}C_3H_7CHO$ molecule, $[i\text{-}C_3H_7CHO]$ = 10.1 ± 0.15 Torr, $[O_2]$ = 80 Torr		
6.0	20.0	0.066
9.8	35.0	0.061
13.8	50.0	0.061
16.0	45.0[a]	0.054
16.4	66.0	0.054
19.5	110.0	0.039
21.3	90.0[a]	0.034
23.5	173.0	0.030
26.1	169.0	0.034

[a] $I_a = 6.6 \times 10^{-4}$ photons min^{-1} per $i\text{-}C_3H_7CHO$ molecule.

occurs as the conversion increases from 6.0 to 26.1 mTorr C_3H_8. However, for conversions below 13.8 mTorr C_3H_8 there is less than 10% fall-off. Comparable data for CO conversions at 312.8 nm are given in Table 3, where it can be seen that the extent of conversion has no effect even for very large conversions.

The effect of pressure on the quantum yields was measured at six incident wavelengths and two temperatures for [*i*-C_3H_7CHO] = 10.0 Torr. The results are shown for C_3H_8 formation in Table 4 and for CO formation in Table 5. For the C_3H_8 measurements, the extent of conversion was kept

TABLE 3

Effect of conversion on CO quantum yield in steady state photolysis[a]

[CO] (mTorr)	*Irradiation time* (min)	Φ(CO)
45.6	10.0	0.88
71.1	15.0	0.92
119.2	25.0	0.91
186.4	40.0	0.89
234.8	50.0	0.90

[a]λ = 312.8 nm, T = 294 K, $I_a = 4.5 \times 10^{-4}$ photons min^{-1} per *i*-C_3H_7CHO molecule, [*i*-C_3H_7CHO] = 10.1 ± 0.1 Torr and [O_2] = 135 Torr.

TABLE 4

Effect of O_2 and N_2 pressure on the C_3H_8 quantum yield in steady state photolysis for [*i*-C_3H_7CHO] = 10.0 ± 0.02 Torr

[O_2] + [N_2] (Torr)	[N_2] (Torr)	*Irradiation time* (min)	Φ(C_3H_8)
λ = 253.7 nm, T = 294 K, $I_a = 1.12 \times 10^{-4}$ photons min^{-1} per i-C_3H_7CHO molecule			
16	0	33.0	0.78
22[a]	0	12.0	0.75
22	0	31.0	0.73
30	0	30.0	0.82
55	0	31.0	0.67
91	0	31.0	0.62
110	0	30.0	0.59
161	0	46.0	0.57
180	0	35.0	0.57
283	0	45.0	0.53
350[a]	328	12.0	0.51
351	0	50.0	0.53
402	0	54.0	0.54
500	0	30.0	0.50
595	0	32.0	0.49
570[a]	548	13.0	0.47
735[a]	713	12.0	0.48

(continued)

TABLE 4 *(continued)*

$[O_2] + [N_2]$ (Torr)	$[N_2]$ (Torr)	*Irradiation time* (min)	$\Phi(C_3H_8)$
λ = 280.3 nm, T = 294 K, I_a = 9.5 × 10^{-5} photons min^{-1} per i-C_3H_7CHO molecule			
15	0	16.0	0.68
15[b]	0	31.0	0.62
50	0	25.0	0.59
85	0	25.0	0.54
157	0	30.0	0.46
240	0	32.0	0.44
255[b]	240	31.0	0.43
330	0	30.0	0.41
430	0	40.0	0.38
490[b]	475	31.0	0.38
530	0	30.0	0.38
680	0	38.0	0.34
695	680	25.0	0.38
710[b]	695	31.0	0.38
λ = 280.3 nm, T = 294 K, I_a = 7.4 × 10^{-5} photons min^{-1} per i-C_3H_7CHO molecule			
40	0	25.0	0.56
131	0	30.0	0.46
255	0	30.0	0.42
298	0	30.0	0.40
400	0	35.0	0.36
496	0	42.0	0.42
645	0	40.0	0.32
λ = 302.2 nm, T = 294 K, I_a = 1.56 × 10^{-5} photons min^{-1} per i-C_3H_7CHO molecule			
28	0	359.0	0.329
80	0	390.0	0.152
112	0	340.0	0.138
190	0	455.0	0.079
311	0	560.0	0.053
λ = 312.8 nm, T = 294 K, I_a = 5.9 × 10^{-4} photons min^{-1} per i-C_3H_7CHO molecule			
22	0	16.0	0.136
46	0	30.0	0.081
80[c]	0	45.0	0.054
80	0	45.0	0.051
187	0	60.0	0.027
188	0	60.0	0.030
279	0	60.0	0.019
316	0	61.0	0.019
441	0	82.0	0.014
555	0	60.0	0.013
560[c]	0	45.0	0.017
695	0	45.0	0.017

(continued)

TABLE 4 *(continued)*

$[O_2] + [N_2]$ (Torr)	$[N_2]$ (Torr)	*Irradiation time* (min)	$\Phi(C_3H_8)$
$\lambda = 312.8$ nm, $T = 294$ K, $I_a = 5.1 \times 10^{-4}$ photons min^{-1} per $i\text{-}C_3H_7CHO$ molecule			
25	0	31.0	0.112
50	0	25.0	0.092
160	0	30.0	0.051
200	0	45.0	0.030
302	0	70.0	0.024
470	0	70.0	0.020
685	0	111.0	0.015
$\lambda = 326.1$ nm, $T = 294$ K, $I_a = 9.8 \times 10^{-5}$ photons min^{-1} per $i\text{-}C_3H_7CHO$ molecule			
22	0	35.0	0.263
22	0	64.0	0.275
70	0	50.0	0.152
70	0	90.0	0.149
140	0	120.0	0.050
145	0	220.0	0.060
150	128	180.0	0.064
200	0	250.0	0.031
252	0	228.0	0.027
365	0	495.0	0.016
$\lambda = 326.1$ nm, $T = 294$ K, $I_a = 7.6 \times 10^{-5}$ photons min^{-1} per $i\text{-}C_3H_7CHO$ molecule			
17	0	55.0	0.315
40	0	85.0	0.185
90	0	120.0	0.142
134	0	200.0	0.055
190	0	211.0	0.032
265	0	215.0	0.028
$\lambda = 334.1$ nm, $T = 294$ K, $I_a = 1.95 \times 10^{-5}$ photons min^{-1} per $i\text{-}C_3H_7CHO$ molecule			
38	0	480.0	0.264
53	0	510.0	0.202
82	0	440.0	0.162
190	0	550.0	0.074
293	0	642.0	0.058
368	0	720.0	0.050
505	0	754.0	0.039
$\lambda = 280.3$ nm, $T = 263$ K, $I_a = 6.1 \times 10^{-5}$ photons min^{-1} per $i\text{-}C_3H_7CHO$ molecule			
15	0	86.0	0.57
32	0	105.0	0.53
58	0	76.0	0.49
61	0	90.0	0.49
95	0	90.0	0.46
130	0	100.0	0.45
210	0	104.0	0.42
305	0	92.0	0.39
405	0	90.0	0.35
505	0	106.0	0.34
640	0	75.0	0.32
640	0	96.0	0.30

(continued)

TABLE 4 *(continued)*

$[O_2] + [N_2]$ (Torr)	$[N_2]$ (Torr)	*Irradiation time* (min)	$\Phi(C_3H_8)$
λ = 312.8 nm, T = 263 K, I_a = 5.1 × 10^{-4} photons min^{-1} per i-C_3H_7CHO molecule			
20	0	35.0	0.112
80	0	40.0	0.074
165	0	51.0	0.043
235	0	40.0	0.043
305	0	55.0	0.041
405	0	55.0	0.030
540	0	61.0	0.026
λ = 326.1 nm, T = 263 K, I_a = 7.8 × 10^{-5} photons min^{-1} per i-C_3H_7CHO molecule			
12	0	70.0	0.170
35	0	85.0	0.123
57	0	110.0	0.103
135	0	163.0	0.070
185	0	190.0	0.053
255	0	240.0	0.044

[a] I_a = 1.74 × 10^{-4} photons min^{-1} per i-C_3H_7CHO molecule.
[b] I_a = 6.6 × 10^{-5} photons min^{-1} per i-C_3H_7CHO molecule.
[c] I_a = 6.6 × 10^{-4} photons min^{-1} per i-C_3H_7CHO molecule.

TABLE 5

Effect of O_2 and N_2 pressure on the CO quantum yield in steady state photolysis for [i-C_3H_7CHO] = 10.0 ± 0.2 Torr

$[O_2]$ (Torr)	*Irradiation time* (min)	Φ(CO)
λ = 253.7 nm, T = 294 K, I_a = 1.12 × 10^{-4} photons min^{-1} per i-C_3H_7CHO molecule		
18	90.0	0.93
34	50.0	0.86
36	95.0	0.88
87	95.0	0.78
113	100.0	0.76
116	85.0	0.76
182	91.0	0.72
212	90.0	0.71
260	85.0	0.72
270	105.0	0.72
282	95.0	0.71
348	120.0	0.67
372	100.0	0.64
400	120.0	0.65
462	102.0	0.65
530	105.0	0.65
660	175.0	0.65

(continued)

TABLE 5 *(continued)*

$[O_2]$ (Torr)	*Irradiation time* (min)	Φ(CO)
λ = 280.3 nm, T = 294 K, I_a = (5.1 ± 0.2) × 10^{-5} photons min^{-1} per i-C_3H_7CHO molecule		
2.78[a]	245.0	1.00[b]
25	200.0	0.84
42	180.0	0.78
80	180.0	0.81
175	190.0	0.79
270	181.0	0.76
385	235.0	0.76
485	245.0	0.75
640	185.0	0.76
λ = 302.2 nm, T = 294 K, I_a = 1.56 × 10^{-5} photons min^{-1} per i-C_3H_7CHO molecule		
16	260.0	0.99[b]
29.5[c]	240.0	0.87
77[d]	348.0	0.80
80	300.0	0.79
115	362.0	0.72
190	310.0	0.62
245	432.0	0.62
262	375.0	0.67
313	426.0	0.58
380	510.0	0.60
390	540.0	0.54
448	518.0	0.51
615	540.0	0.53
λ = 312.8 nm, T = 294 K, I_a = 5.9 × 10^{-4} photons min^{-1} per i-C_3H_7CHO molecule		
8.6	20.0	1.05
26.3	21.0	1.04
42	20.0	0.98
80	20.0	0.96
115	20.0	0.96
126	20.0	0.98
165[d]	20.0	0.94
190	20.0	0.87
277	20.0	0.92
314	20.0	0.96
438	20.0	0.91
480[d]	20.0	0.89
552	21.0	0.86
637	20.0	0.88
λ = 326.1 nm, T = 294 K, I_a = 6.7 × 10^{-5} photons min^{-1} per i-C_3H_7CHO molecule		
22	205.0	0.98
55	185.0	0.89
95	180.0	0.86
122	185.0	0.88
178	212.0	0.91
210	190.0	0.88

(continued)

TABLE 5 *(continued)*

$[O_2]$ (Torr)	*Irradiation time* (min)	Φ(CO)
250	255.0	0.88
292	210.0	0.79
315	181.0	0.80
405	195.0	0.85
495	286.0	0.78
565	220.0	0.78
580	205.0	0.79
λ = 334.1 nm, T = 294 K, $I_a = 1.95 \times 10^{-5}$ photons min^{-1} per i-C_3H_7CHO molecule		
20.8	360.0	1.08
28.8	380.0	1.03
50	479.0	0.95
82	450.0	0.94
117	430.0	0.91
191	485.0	0.83
292	480.0	0.75
363	494.0	0.73
502	490.0	0.71
λ = 280.3 nm, T = 263 K, $I_a = 7.0 \times 10^{-5}$ photons min^{-1} per i-C_3H_7CHO molecule		
15	86.0	0.92
32	105.0	0.85
58	76.0	0.92
95	90.0	0.83
130	100.0	0.92
210	104.0	0.87
305	92.0	0.91
405	90.0	0.84
505	106.0	0.87
λ = 312.8 nm, T = 263 K, $I_a = 5.1 \times 10^{-4}$ photons min^{-1} per i-C_3H_7CHO molecule		
17	15.0	0.99
22	15.0	0.97
39	15.0	0.98
55	21.0	0.93
77	18.0	0.91
130	18.0	0.91
210	28.0	0.84
315	20.0	0.87
412	20.0	0.83
530	20.0	0.78
λ = 326.1 nm, T = 263 K, $I_a = 7.8 \times 10^{-5}$ photons min^{-1} per i-C_3H_7CHO molecule		
10	159.0	0.77
35	145.0	0.79
55	196.0	0.71
85	187.0	0.70
90	170.0	0.69
138	181.0	0.67

(continued)

TABLE 5 *(continued)*

$[O_2]$ (Torr)	*Irradiation time* (min)	$\Phi(CO)$
205	188.0	0.66
240	180.0	0.61
320	217.0	0.53
325	190.0	0.61
400	230.0	0.51
525	240.0	0.51
642	245.0	0.48

[a] $[i\text{-}C_3H_7CHO] = 6.34$ Torr, $I_a = 6.5 \times 10^{-5}$ photons min^{-1} per $i\text{-}C_3H_7CHO$ molecule.
[b] Assumed value.
[c] $[i\text{-}C_3H_7CHO] = 10.5$ Torr.
[d] Diluent is dry air rather than O_2.

low (below 12 mTorr at all wavelengths except 253.7 nm) to be sure that initial quantum yields were being measured. At all wavelengths both $\Phi(C_3H_8)$ and $\Phi(CO)$ fall with increasing pressure, though $\Phi(CO)$ at all wavelengths and $\Phi(C_3H_8)$ at 253.7 and 280.3 nm reach lower limiting values.

The effect of O_2 pressure on $\Phi(C_3H_8)$ at 312.8 nm, 294 K and $[i\text{-}C_3H_7CHO] = 31.1$ Torr is given in Table 6. As at lower $i\text{-}C_3H_7CHO$ pressure, $\Phi(C_3H_8)$ falls as $[O_2]$ increases. However, at any O_2 pressure $\Phi(C_3H_8)$ is larger at 31 Torr than at 10.0 Torr $i\text{-}C_3H_7CHO$. This is shown more clearly in Table 7 which gives the results from a series of runs at constant O_2 pressure, but with various $i\text{-}C_3H_7CHO$ pressures at 294 K and 312.8 nm. $\Phi(C_3H_8)$ increases dramatically with increasing $i\text{-}C_3H_7CHO$ pressure. In contrast, $\Phi(CO)$ is not affected at all, as shown in Table 8.

TABLE 6

Effect of O_2 pressure on the C_3H_8 quantum yield in steady state photolysis for $[i\text{-}C_3H_7CHO] = 31.1 \pm 0.1$ Torr at 312.8 nm and 294 K[a]

$[O_2]$ (Torr)	*Irradiation time* (min)	$\Phi(C_3H_8)$
29	3.00	0.54
94	3.00	0.41
184	3.00	0.40
217	3.50	0.40
274	4.00	0.35
349	3.00	0.34
381	3.00	0.32
475	4.00	0.31
587	4.00	0.24
614[b]	4.00	0.26

[a] $I_a = (2.72 \pm 0.02) \times 10^{14}$ photons cm^{-3} min^{-1}.
[b] $[O_2] = 22$ Torr; $[N_2] = 592$ Torr.

TABLE 7

Effect of i-C_3H_7CHO pressure on the C_3H_8 quantum yield in steady state photolysis for $[O_2]$ = 23 Torr at 312.8 nm and 294 K

$[i\text{-}C_3H_7CHO]$ (Torr)	$[O_2]$ (Torr)	*Irradiation time* (min)	$I_a \times 10^{-14}$ (photons cm^{-3} min^{-1})	$\Phi(C_3H_8)$
1.69	19	322.00	0.197	0.048
2.70	23	280.00	0.31	0.064
4.80	26	32.00	0.56	0.109
5.08	23	55.00	0.59	0.105
10.15	18	15.00	1.10	0.197
19.83	10	8.00	1.95	0.28
20.11	20	8.00	1.98	0.24
23.61	22	4.50	2.18	0.35
28.65	22	4.00	2.55	0.36
33.88	22	3.00	2.84	0.57
36.99	22	3.00	2.95	0.61
38.17	22	2.00	3.00	0.90
38.20	23	2.00	3.00	0.92
39.19	21	2.00	3.10	1.09
39.86	23	2.00	3.08	0.79

TABLE 8

Effect of i-C_3H_7CHO pressure on the CO quantum yield in steady state photolysis for $[O_2]$ = 23 Torr at 312.8 nm and 294 K

$[i\text{-}C_3H_7CHO]$ (Torr)	$[O_2]$ (Torr)	*Irradiation time* (min)	$I_a \times 10^{-14}$ (photons cm^{-3} min^{-1})	$\Phi(CO)$
1.69	20	322.0	0.197	1.02
5.00	20	85.0	0.58	1.09
35.6	24	10.0	3.06	1.10

The data for $\Phi(C_3H_8)$ at constant i-C_3H_7CHO pressure are fitted to the Stern–Volmer function

$$\{\Phi(C_3H_8) - \Phi(C_3H_8)_\infty\}^{-1} = \frac{1 + \beta[M]}{\alpha} \qquad (I)$$

where $\Phi(C_3H_8)_\infty$ is the high pressure limiting value of $\Phi(C_3H_8)$, α and β are constant at any i-C_3H_7CHO pressure and $[M] = [O_2] + [N_2]$. The left-hand side of eqn. (I) was calculated using the extrapolated values $\Phi(C_3H_8)_\infty = 0.43$ at 253.7 nm, $\Phi(C_3H_8)_\infty = 0.31$ at 280.3 nm and $\Phi(C_3H_8)_\infty = 0.0$ at other wavelengths. Plots of this function *versus* $[O_2] + [N_2]$ are given in Figs. 1 - 3 at the various wavelengths and both temperatures. The data for the three wavelengths where data were obtained only at 294 K are shown in

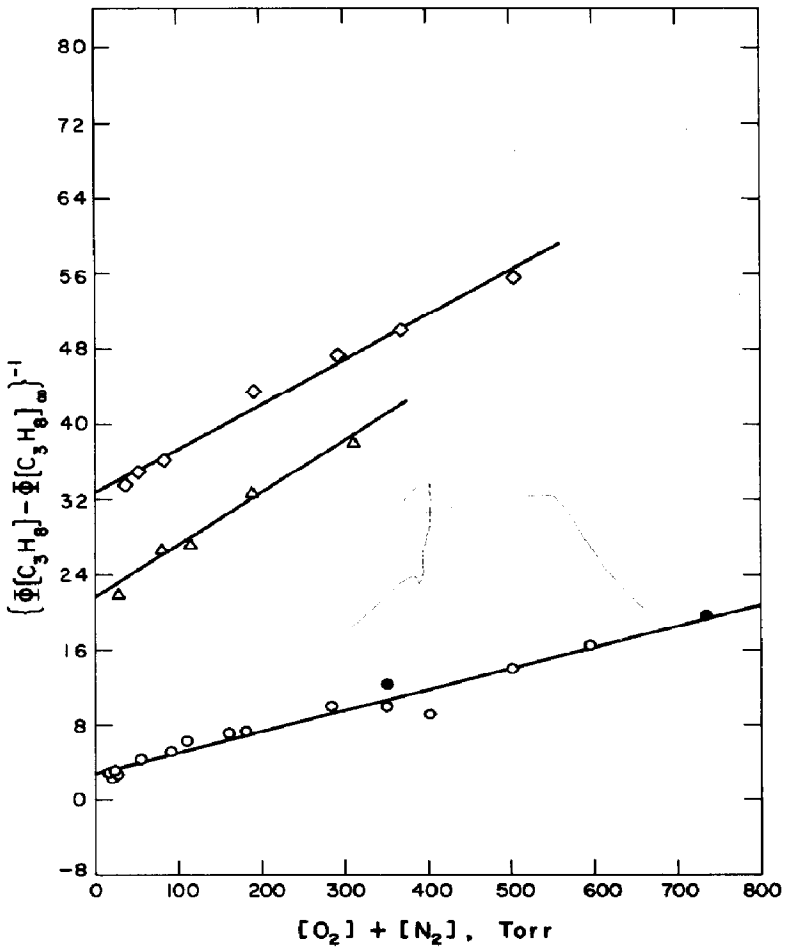

Fig. 1. Plots of $\{\Phi(C_3H_8)-\Phi(C_3H_8)_\infty\}^{-1}$ *vs.* $[O_2]+[N_2]$ at 294 K for $[i\text{-}C_3H_7CHO]$ = 10.0 Torr: ○, 253.7 nm; △, 302.2 nm; ◇, 334.1 nm. The full symbols are for data where N_2 is present; the open symbols are where N_2 is absent. The plots at 302.2 and 334.1 nm are displaced upward by 20 and 30 units respectively, for clarity.

Fig. 1. They all give reasonable straight-line plots. The least-squares values of their intercepts $1/\alpha$ and slopes β/α are given in Table 9.

The data for 312.8 and 326.1 nm are plotted in Fig. 2. At 312.8 nm, the data at 263 K are the same as those at 294 K at low $[O_2]+[N_2]$, but lie lower at higher $[O_2]+[N_2]$. However, there is so much scatter in the data that it is difficult to tell whether this difference is real. For simplicity, we fitted all the data to one straight-line plot whose least-squares intercept and slope are listed in Table 9. The low temperature data at 326.1 nm give a linear plot. However, the data at 294 K show curvature. We do not understand the reason for this curvature, so again, for simplicity, we have based the least-squares line on the low temperature data only.

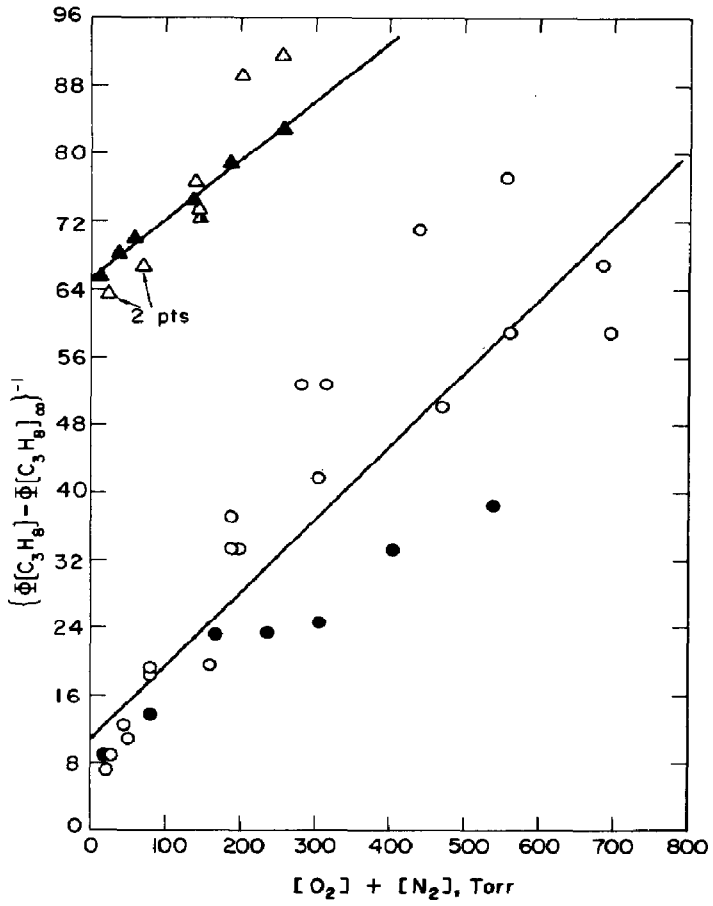

Fig. 2. Plots of $\{\Phi(C_3H_8) - \Phi(C_3H_8)_\infty\}^{-1}$ *vs.* $[O_2] + [N_2]$ for $[i\text{-}C_3H_7CHO]$ = 10.0 Torr: ○, 312.8 nm; △, 326.1 nm. Open symbols, 294 K; full symbols, 263 K; half-full symbols, N_2 present at 294 K. The plot at 326.1 nm is displaced upward by 60 units for clarity.

The data at 280.3 nm at both temperatures lie on the same line, as shown in Fig. 3. Also shown in Fig. 3 are the data at 312.8 nm with $[i\text{-}C_3H_7CHO]$ = 31.1 Torr. They also give a good straight-line plot.

From the data in Table 7, we see that $\Phi(C_3H_8)$ increases with i-C_3H_7CHO pressure. Therefore we have fitted it to an inverse Stern–Volmer plot and plotted $\Phi(C_3H_8)^{-1}$ *vs.* $[i\text{-}C_3H_7CHO]^{-1}$ in Fig. 4. The data can be fitted by a straight line whose least-squares intercept and slope are 1.12 ± 0.32 and 35.8 ± 1.6 Torr respectively, where the uncertainties are one standard deviation.

As already stated, the radical quantum yield Φ(rad) is given by

$$\Phi(\text{rad}) = \Phi(CO) - \Phi(C_3H_8) \qquad \text{(II)}$$

These are calculated using the experimentally measured values of Φ(CO) and the values for $\Phi(C_3H_8)$ computed from the Stern–Volmer plots in Figs. 1 - 3.

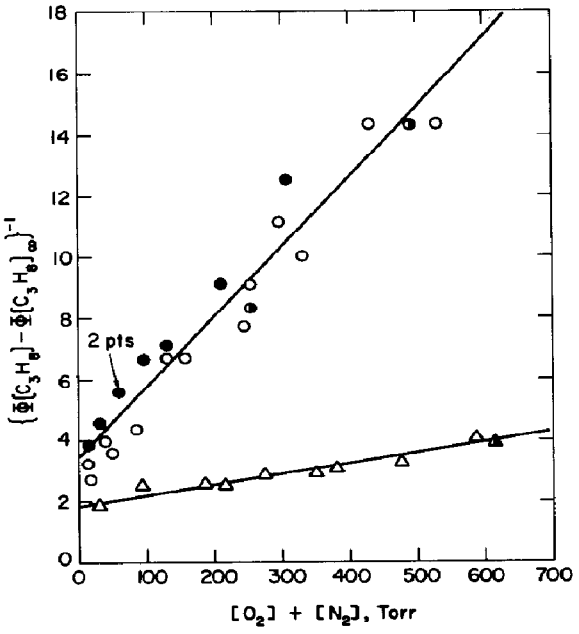

Fig. 3. Plots of $\{\Phi(C_3H_8) - \Phi(C_3H_8)_\infty\}^{-1}$ *vs.* $[O_2] + [N_2]$: ○, 280.3 nm, $[C_3H_7CHO]$ = 10.0 Torr; △, 312.8 nm, $[C_3H_7CHO]$ = 31.1 Torr. Open symbols, 294 K; full symbols, 263 K; half-full symbols, N_2 present at 294 K.

TABLE 9

Analysis of C_3H_8 data for $[i\text{-}C_3H_7CHO]$ = 10.0 Torr[a]

λ (nm)	T (K)	$\Phi(C_3H_8)_\infty$	$1/\alpha$	$10^2\beta/\alpha$ (Torr^{-1})	α	$1/\beta$ (Torr)
253.7	294	0.43	2.84 ± 0.38	2.24 ± 0.12	0.35 ± 0.05	127 ± 22
280.3	Both	0.31	3.43 ± 0.31	2.28 ± 0.13	0.29 ± 0.03	150 ± 21
302.2	294	0.00	1.61 ± 0.04	5.60 ± 0.24	0.62 ± 0.01	29 ± 9
312.8	Both	0.00	10.8 ± 3.4	8.65 ± 0.98	0.093 ± 0.029	125 ± 51
312.8	294[b]	0.00	1.87 ± 0.12	0.34 ± 0.03	0.53 ± 0.03	550 ± 82
326.1	263	0.00	5.48 ± 0.35	6.9 ± 0.2	0.18 ± 0.01	79 ± 8
334.1	294	0.00	2.78 ± 0.65	4.7 ± 0.2	0.36 ± 0.08	59 ± 16

[a] All uncertainties are one standard deviation.
[b] $[i\text{-}C_3H_7CHO]$ = 31.1 Torr.

The values of Φ(rad) are also fitted to the Stern–Volmer plots

$$\Phi(\text{rad})^{-1} = \frac{1 + \delta[M]}{\gamma} \qquad \text{(III)}$$

where γ and δ are constants at any $i\text{-}C_3H_7CHO$ pressure and $[M] = [O_2] + [N_2]$.

The Φ(rad) are essentially invariant to [M] at 253.7 and 280.3 nm, within the experimental uncertainty of the data. They are 0.15 ± 0.02 at 253.7 nm and 294 K, 0.34 ± 0.05 at 280.3 nm and 294 K and 0.45 ± 0.07 at

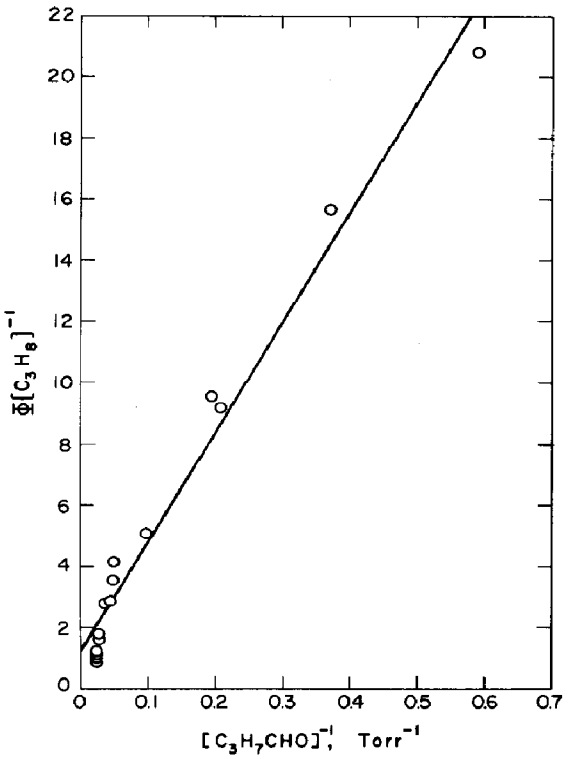

Fig. 4. Plot of $\Phi(C_3H_8)^{-1}$ *vs.* $[i\text{-}C_3H_7CHO]^{-1}$ for $[O_2]$ = 23 Torr at 294 K and 312.8 nm.

280.3 nm and 263 K. At the other wavelengths they are plotted *versus* $[O_2] + [N_2]$ in Fig. 5. All of the plots are linear. Their least-squares intercepts $1/\gamma$ and slopes δ/γ are listed in Table 10. At 312.8 and 326.1 nm, the data at low temperature lie above those at high temperature, though the effect is much greater at 326.1 nm than at 312.8 nm.

3.2. Flash photolysis

Flash photolysis of $i\text{-}C_3H_7CHO$–air, or Cl_2–O_2–C_3H_8 mixtures, with the laser produces a transient absorption at 250 nm. A sample absorption trace is shown in Fig. 6. After the flash, the absorption remains constant for a considerable time. For the $i\text{-}C_3H_7CHO$–air mixture, if we assume that the observed absorption is attributed solely to $i\text{-}C_3H_7O_2$, then we can compute the relative quantum yields $\Phi_{rel}(rad)$. These values are listed in Table 11 as a function of air pressure and incident wavelength. Pressure variations were made only at 311.7 and 330.5 nm. In accordance with the findings of the steady state photolysis, there is no pressure quench at 311.7 nm. However, at 330.5 nm a slight pressure quench exists. The Stern–Volmer plot of $\Phi_{rel}(rad)^{-1}$ *versus* total pressure [M] is shown in Fig. 7. The intercept is 0.62 ± 0.02 and the slope is $(2.5 \pm 0.6) \times 10^{-4}$ Torr^{-1}. The ratio of the slope to the intercept gives $k_6/k_5 = (4.0 \pm 1.0) \times 10^{-4}$ Torr^{-1}. The reported uncertainties are one standard deviation.

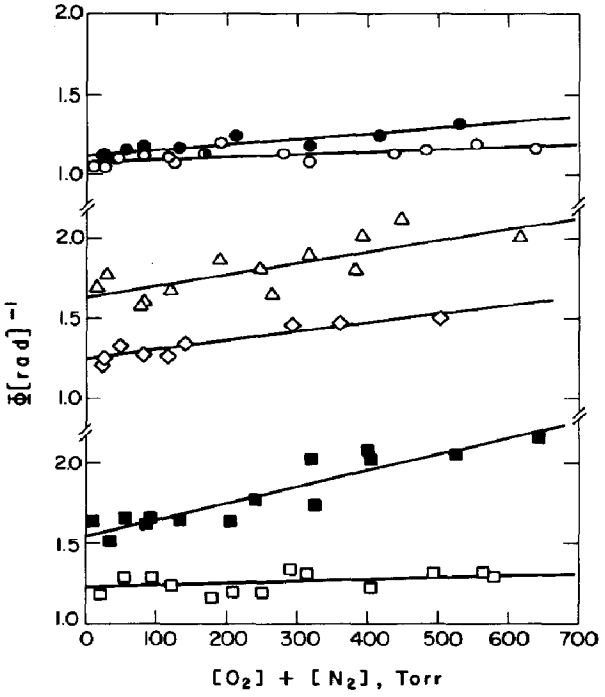

Fig. 5. Plots of $\Phi(\text{rad})^{-1}$ as calculated from eqn. (II) *vs.* $[O_2] + [N_2]$ for $[i\text{-}C_3H_7CHO] = 10.0$ Torr: △, 302.2 nm; ○, 312.8 nm; □, 326.1 nm; ◇, 334.1 nm. Open symbols, 294 K; full symbols, 263 K; half-full symbols, N_2 present at 294 K.

For the four incident wavelengths where the values of $\Phi_{rel}(\text{rad})$ can be compared they are 0.63 ± 0.04 (284.0 nm), 1.20 ± 0.04 (302.5 nm), 1.52 ± 0.15 (325.0 nm) and 1.62 ± 0.06 (330.5 nm), where the value at 330.5 nm is the low-air-pressure limiting value.

4. Discussion

The results here are consistent with the mechanism given by reactions (1) - (6) with an important modification. $i\text{-}C_3H_7CHO$ does not quench $\Phi(CO)$ and enlarges $\Phi(C_3H_8)$. This cannot be due to competition between $i\text{-}C_3H_7CHO$ and O_2 for the $i\text{-}C_3H_7$ radical, because replacing part of the O_2 by N_2 does not change $\Phi(C_3H_8)$. Thus $i\text{-}C_3H_7CHO$ must act to convert the radical-forming step to the molecular elimination step. Consequently we consider M to be only O_2 and N_2 in reactions (4) and (6) and treat $i\text{-}C_3H_7CHO$ separately.

The quenching by $i\text{-}C_3H_7CHO$ must proceed as follows:

$$A_n + A \longrightarrow A + \text{removal of } A_n \qquad (7)$$

$$^3A_n + A \longrightarrow A_n + A \qquad (8a)$$

$$\longrightarrow {}^3A_0 + A \qquad (8b)$$

TABLE 10

Analysis of radical yield data from steady state photolysis for [i-C_3H_7CHO] = 10 Torr[a]

λ (nm)	T (K)	$\Phi(CO)_0$[b]	$1/\gamma$	$10^4\delta/\gamma$ (Torr)	γ	$10^{-4}/\delta$ (Torr)	$\alpha + \gamma + \Phi(C_3H_8)_\infty$	k_5/k_6 (Torr)
253.7	294	0.95	—	—	0.15 ± 0.02	—	0.93	—
280.3	294	1.00[c]	—	—	0.34 ± 0.05	—	0.94	—
280.3	263	1.00[c]	—	—	0.45 ± 0.07	—	1.05	—
302.2	294	1.00[c]	1.63 ± 0.05	7.1 ± 1.7	0.61 ± 0.02	0.23 ± 0.06	1.23	1700
312.8	294	1.10	1.07 ± 0.02	1.6 ± 0.5	0.93 ± 0.02	0.67 ± 0.24	1.02	5100
312.8	263	1.00	1.12 ± 0.01	3.4 ± 0.6	0.89 ± 0.01	0.33 ± 0.06	0.98	2500
326.1	294	1.00	1.21 ± 0.03	1.6 ± 0.8	0.83 ± 0.03	0.76 ± 0.38	1.01	5800
326.1	263	0.80	1.55 ± 0.04	10.0 ± 1.3	0.64 ± 0.02	0.155 ± 0.020	0.82	1200
334.1	294	1.10	1.24 ± 0.02	5.5 ± 0.8	0.81 ± 0.02	0.23 ± 0.03	1.17	1700

[a] All uncertainties are one standard deviation.

[b] Extrapolated from experimental data by plotting $\{\Phi(CO) - \Phi(CO)_\infty\}^{-1}$ *versus* $[O_2] + [N_2]$. These values should all be unity; actual values represent errors in actinometry.

[c] Assumed.

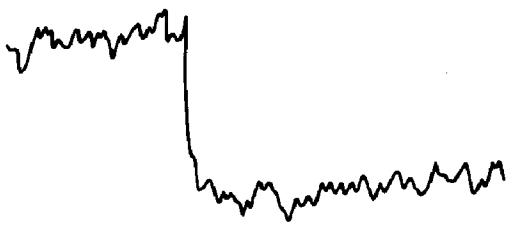

Fig. 6. Plot of light intensity at 250 nm *vs.* time after the flash in the 330.5 nm photolysis of a mixture of i-C_3H_7CHO at 32.9 Torr and air at 14.6 Torr. The time scale runs from left to right with a sweep time of 2 μs per channel. The fraction of light absorbed is 0.0050. The plot is an average of 32 shots.

TABLE 11

Flash photolysis of i-C_3H_7CHO in air: relative quantum yields or i-$C_3H_7O_2$ formation at 298 ± 2 K

Total pressure (Torr)	[i-C_3H_7CHO] (Torr)	E [a]	N [b]	Φ_{rel}(rad)
λ = *284.0 ± 0.3 nm*				
44.2	15.0	0.168	32	0.65
44.2	15.0	0.150	32	0.66
44.2	15.0	0.140	32	0.65
45.1	14.9	0.282	32	0.56
45.1	14.9	0.202	32	0.58
45.1	14.9	0.152	32	0.62
45.8	14.9	0.165	16	0.62
45.8	14.9	0.165	16	0.68
45.8	14.9	0.120	32	0.67
λ = *302.5 ± 0.3 nm*				
44.3	15.0	0.200	8	1.19
44.3	15.0	0.211	8	1.22
44.3	15.0	0.214	8	1.23
44.3	15.0	0.230	8	1.18
44.6	15.1	0.218	8	1.22
44.6	15.1	0.230	8	1.26
44.6	15.1	0.245	8	1.26
44.6	15.1	0.243	8	1.15
46.4	15.0	0.250	8	1.17
46.4	15.0	0.263	8	1.17
46.4	15.0	0.247	8	1.16
46.4	15.0	0.257	8	1.17
λ = *311.7 ± 0.3 nm* [c]				
43.2	15.2	0.147	16	5.18
43.2	15.2	0.135	16	5.50
43.8	15.3	0.140	16	5.81
43.8	15.3	0.158	16	5.62
44.9	15.3	0.117	16	4.98
44.9	15.3	0.105	16	5.38

(continued)

TABLE 11 *(continued)*

Total pressure (Torr)	[i-C_3H_7CHO] (Torr)	E [a]	N [b]	Φ_{rel}(rad)
45.4	15.5	0.131	16	5.16
45.4	15.5	0.115	16	5.16
250	15.3	0.152	16	5.10
250	15.3	0.140	16	5.24
299	15.5	0.130	16	5.71
299	15.5	0.139	16	5.65
355	15.3	0.134	16	4.88
445	15.2	0.137	16	4.90
445	15.2	0.115	16	5.00
584	15.2	0.129	16	4.83
584	15.2	0.130	16	5.16
598	15.5	0.131	16	5.35
653	15.3	0.136	16	4.85
653	15.3	0.139	16	5.21
λ = *325.0 ± 0.3 nm*				
46.3	25.4	0.121	32	1.62
46.3	25.4	0.123	32	1.54
47.9	24.6	0.141	32	1.72
47.9	24.6	0.134	32	1.54
49.5	25.1	0.128	32	1.37
49.5	25.1	0.128	32	1.33
λ = *330.5 ± 0.3 nm*				
46.4	30.0	0.122	32	1.70
46.4	30.0	0.124	32	1.78
47.5	32.9	0.116	32	1.36
99.4	30.4	0.105	32	1.62
99.4	30.4	0.108	32	1.46
271	30.0	0.117	32	1.52
327	30.4	0.102	32	1.40
667	31.8	0.250	32	1.32
667	31.8	0.228	32	1.27
674	32.9	0.113	32	1.22

[a] Average relative energy per shot.
[b] Number of laser shots.
[c] These relative quantum yields were obtained from the signal-to-power ratios. No actinometry runs were done at this wavelength. Therefore they cannot be compared directly with data at other wavelengths.

Under our conditions, $\Phi(CO)$ is not reduced by increasing the i-C_3H_7CHO pressure. Thus k_7 should be small and reaction (7) can be ignored. Reaction (8b) is necessary to account for the enhanced biacetyl phosphorescence seen by Borkowski and Ausloos [45] with increasing [i-C_3H_7CHO]. However it must be very small compared with reaction (8a), since $\Phi(CO)$ is not reduced below 1.0 at high i-C_3H_7CHO pressure. For the purpose of this discussion reaction (8b) can be neglected.

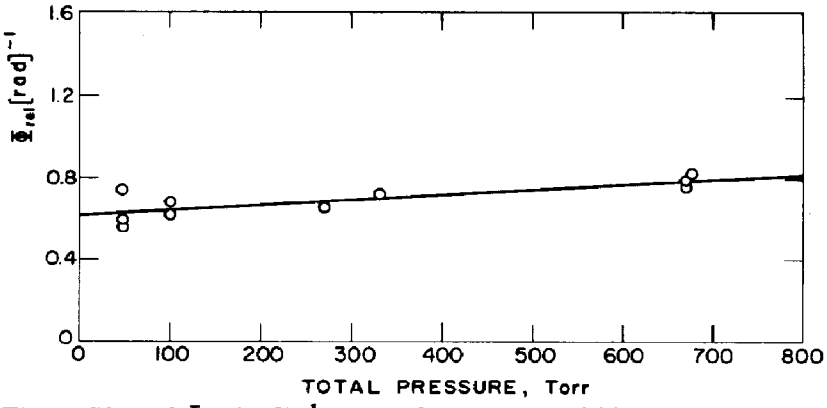

Fig. 7. Plot of $\Phi_{rel}(rad)^{-1}$ *vs.* total pressure at 330.5 nm.

In principle, O_2 and N_2 might also quench ^3A_n to A_n. However, quenching of ^3A_n by O_2 and N_2 is so small under our conditions, *i.e.* Φ(rad) is not greatly affected by changing $[O_2]$ or $[N_2]$, that we cannot tell whether this occurs. For simplicity in the analysis, we ignore the possibility. Also, the data in Table 7 indicate that $\Phi(C_3H_8)$ approaches 0.00 at low *i*-C_3H_7CHO pressure. This requires that reaction (2b) be negligible, at least at 312.8 nm. Again for simplicity, we shall ignore reaction (2b) at all wavelengths.

The mechanism then consists of reactions (1), (2a), (2c), (2d), (3) - (7) and (8a). This mechanism leads to the rate law

$$\Phi(C_3H_8)_\infty = \frac{k_{2a}}{k_2} \qquad \text{(IV)}$$

as well as to the rate laws given by eqns. (I) (omitting reactions (6) and (7)) and (III) with

$$\alpha \equiv \frac{(k_{2c}/k_2)k_8[A]/k_5}{1 + k_8[A]/k_5}$$

$$\beta \equiv \frac{k_4}{k_3}$$

$$\gamma = \frac{k_{2c}/k_2}{1 + k_8[A]/k_5}$$

$$\delta = \frac{k_6/k_5}{1 + k_8[A]/k_5}$$

From these definitions we can see that $\alpha + \gamma = k_{2c}/k_2$ and that

$$\Phi(CO)_0 = \alpha + \gamma + \Phi(C_3H_8)_\infty \qquad \text{(V)}$$

where $\Phi(CO)_0$ is the limiting low pressure value of Φ(CO). Values of the right-hand side of eqn. (V) are listed in Table 10 and they do agree with $\Phi(CO)_0$ to within the experimental uncertainty.

With reactions (6) and (7) omitted the rate law also gives

$$\{\Phi(C_3H_8) - \Phi(C_3H_8)_\infty\}^{-1} = (1 + \beta[M])(k_2/k_{2c})(1 + k_5/k_8[A]) \quad \text{(VI)}$$

For [M] = 23 Torr at 312.8 nm (data in Table 7), $\beta[M] \ll 1$, so that a plot of the left-hand side of eqn. (VI) *versus* $[i\text{-}C_3H_7CHO]^{-1}$ gives a straight line (Fig. 4) with an intercept $k_2/k_{2c} = 1.12 \pm 0.32$ and slope $(k_2/k_{2c})(k_5/k_8) = 35.8 \pm 1.6$ Torr. Thus at 312.8 nm $k_{2c}/k_2 = 0.89$ and $k_5/k_8 = 32.1 \pm 10.0$ Torr. The latter value is in good agreement with the half-quenching pressure of about 40 Torr found by Borkowski and Ausloos [45] at 334.1 nm and 306 K.

The half-quenching pressure k_5/k_6 for O_2 and N_2 can be found from δ and $k_5/k_8 = 32.1$ Torr, which we assume to be independent of temperature and incident wavelength. Actually k_5/k_8 should be a function of incident wavelength, but for [A] = 10 Torr, $1 + k_8[A]/k_5$ will not differ greatly from 1.0. The computed values of k_5/k_6 are listed in Table 10. There is no measurable quenching at 253.7 or 280.3 nm, and k_5/k_6 is very large. It decreases as the radiation energy or temperature drops, as expected, except for the value at 302.2 nm which is anomalously low.

In principle, k_3/k_4 can be found at 312.8 nm from

$$1/\beta \equiv k_3/k_4 \quad \text{(VII)}$$

The values of $1/\beta$ are 125 Torr and 550 Torr at 10.0 Torr i-C_3H_7CHO and 31.1 Torr i-C_3H_7CHO respectively, indicating that quenching by i-C_3H_7CHO through reaction (7) plays some role. However, there is sufficient uncertainty in the values of $1/\beta$, especially at 10.0 Torr i-C_3H_7CHO, that k_7/k_4 cannot be reasonably estimated. An expected value of k_7/k_4 of about 5 - 10 could be consistent with the data, within the experimental uncertainty. However, since increasing [A] does not reduce $\Phi(CO)$, any quenching by reaction (7) would have to be chemical in nature and lead to CO as a product.

The values of $1/\beta$ listed in Table 9 for $[i\text{-}C_3H_7CHO] = 10.0$ Torr show surprisingly little systematic variation with radiation energy. This suggests that the vibrational level of A_n produced in reaction (8a) is insensitive to the incident energy input.

The values for the radical quantum yield extrapolated to zero pressure of all gases, $\Phi(rad)_0$, can be obtained in three ways. From the steady state photolysis $\Phi(rad)_0 = \alpha + \gamma$ if it is assumed that all the C_3H_8 comes from either ^1A_n or from quenching of ^3A_n by i-C_3H_7CHO. Alternatively, $\Phi(rad)_0$ can be computed from γ alone, assuming an i-C_3H_7CHO half-quenching pressure for ^3A_n of 32.1 Torr at all wavelengths. Relative values of $\Phi(rad)_0$ can be obtained from the flash photolysis results with the same assumption about the half-quenching pressure of i-C_3H_7CHO for ^3A_n. The values computed by all three methods are listed in Table 12. At the higher wavelengths, all three methods are consistent with $\Phi(rad)_0 = 1.0$. At the lower wavelengths the computation of $\Phi(rad)_0 = \alpha + \gamma$ gives the largest values. This suggests that there may be another path (reaction (2b)) to producing A_n,

TABLE 12

Values $\Phi(\text{rad})_0$ of $\Phi(\text{rad})$ extrapolated to zero pressure for all gases at 298 K

λ (nm)	$\Phi(\text{rad})_0$ [a]	$\Phi(\text{rad})_0$ [b]	$\Phi(\text{rad})_0$ [c]
253.7	0.50	0.20	—
280.3	0.63	0.45	—
284.0	—	—	0.36
302.2	1.23	0.80	—
302.5	—	—	0.68
312.8	1.02	1.22	—
325.0	—	—	1.04
326.1	1.01	1.09	—
330.5	—	—	1.20
334.1	1.17	1.06	—

[a] Absolute quantum yields from steady state photolysis assuming $\Phi(\text{rad})_0 = \alpha + \gamma$.
[b] Absolute quantum yields from steady state photolysis extrapolated from γ assuming an i-C_3H_7CHO half-quenching pressure for ^3A_n of 32.1 Torr at all wavelengths.
[c] Normalized relative quantum yields from flash photolysis assuming an i-C_3H_7CHO half-quenching pressure for ^3A_n of 32.1 Torr at all wavelengths. $\Phi(\text{rad})_0$ was normalized to about 1.0 at 313 nm.

which does not go through the triplet state. The values computed from the flash photolysis results show the largest $\Phi(\text{rad})_0$ fall-off with decreasing pressure but otherwise fit the trend given by the steady state photolysis results. The discrepancy may reflect the fact that the aldehyde half-quenching pressure used in the calculation should not be the same at all wavelengths.

5. Atmospheric implication

One goal of this work was to calculate the photodissociation rate coefficient for radical production under atmospheric conditions. This rate coefficient k_{rad} is given by

$$k_{\text{rad}} = \int I_0 \sigma \Phi(\text{rad})\, d\lambda \qquad \text{(VIII)}$$

where I_0 is the incident photon flux at each wavelength λ and σ is the reaction cross section at each wavelength. Values for $\Phi(\text{rad})$ at atmospheric pressure at each wavelength examined in this study are listed in Table 13. The $\Phi(\text{rad})$ at other wavelengths are estimated from a smooth curve through these data.

Values of σ, $\Phi(\text{rad})$ and I_0 at two zenith angles χ over various wavelength intervals are given in Table 14. With these data k_{rad} is computed to be $7.6 \times 10^{-5}\ s^{-1}$ at $\chi = 30°$ and $5.9 \times 10^{-5}\ s^{-1}$ at $\chi = 58.18°$.

TABLE 13

Φ(rad) in air at 1 atm and 294 K for [i-C_3H_7CHO] → 0

λ (nm)	Φ(rad) [a]
253.7	0.20
280.3	0.45
302.2	0.55
312.8	0.88
326.1	0.88
334.1	0.69

[a]Calculated at 1 atm $O_2 + N_2$ using values of k_5/k_6 in Table 10 and $\Phi(rad)_0$ in Table 12 computed by method b.

TABLE 14

Data for evaluating atmospheric photodissociation rate coefficients for i-C_3H_7CHO

λ (nm)	σ [a] (cm^2 $molecule^{-1}$)	Φ(rad) [b]	I_0 [c] (photons cm^{-2} s^{-1})	
			$\chi = 30°$	$\chi = 58.18°$
335.0 - 340.0	2.86×10^{-21}	0.61	1.119×10^{15}	1.081×10^{15}
330.0 - 335.0	6.68×10^{-21}	0.75	1.039×10^{15}	9.883×10^{14}
325.0 - 330.0	1.43×10^{-20}	0.85	1.075×10^{15}	9.928×10^{14}
320.0 - 325.0	2.14×10^{-20}	0.88	8.309×10^{14}	7.289×10^{14}
315.0 - 320.0	2.96×10^{-20}	0.88	6.109×10^{14}	4.847×10^{14}
310.0 - 315.0	3.90×10^{-20}	0.86	4.154×10^{14}	2.803×10^{14}
307.7 - 310.0	4.43×10^{-20}	0.78	2.327×10^{14}	1.088×10^{14}
303.0 - 307.7	4.96×10^{-20}	0.66	7.330×10^{13}	1.771×10^{13}
298.5 - 303.0	5.54×10^{-20}	0.56	9.368×10^{12}	7.001×10^{11}
294.1 - 298.5	5.88×10^{-20}	0.52	4.315×10^{11}	4.273×10^{9}
289.9 - 294.1	5.92×10^{-20}	0.51	2.566×10^{9}	8.83×10^{5}

[a]From Calvert and Pitts [55].
[b]From smooth curve of data in Table 13.
[c]From Wuebbles [57].

Acknowledgment

This work was supported through Grant ATM-8211603 from the Atmospheric Sciences Section of the National Science Foundation for which we are grateful.

References

1 J. E. Carruthers and R. G. W. Norrish, *J. Chem. Soc.*, (1936) 1036.
2 E. C. A. Horner and D. W. G. Style, *Trans. Faraday Soc.*, *50* (1954) 1197.

3 T. C. Purcell and I. R. Cohen, *Environ. Sci. Technol., 1* (1967) 845.
4 J. J. Bufalini and K. L. Brubaker, in C. Tuesday (ed.), *Chemical Reactions in Urban Atmospheres*, Elsevier, New York, 1971, p. 225.
5 R. G. Miller and E. K. C. Lee, *Chem. Phys. Lett., 27* (1974) 475.
6 P. L. Houston and C. B. Moore, *J. Chem. Phys., 65* (1976) 757.
7 T. L. Osif, *Ph.D. Dissertation*, The Pennsylvania State University, 1976.
8 P. Avouris, W. M. Gelbart and M. A. El-Sayed, *Chem. Rev., 77* (1977) 793.
9 F. Su, A. Horowitz and J. G. Calvert, *Int. J. Chem. Kinet., 10* (1978) 1099.
10 J. R. Sodeau and E. K. C. Lee, *Chem. Phys. Lett., 57* (1978) 71.
11 A. Horowitz and J. Calvert, *Int. J. Chem. Kinet., 10* (1978) 713.
12 A. Horowitz and J. Calvert, *Int. J. Chem. Kinet., 10* (1978) 805.
13 J. H. Clark, C. B. Moore and N. S. Nogar, *J. Chem. Phys., 68* (1978) 1264.
14 R. S. Lewis and E. K. C. Lee, *J. Phys. Chem., 82* (1978) 249.
15 G. K. Moortgat, F. Slemr, W. Seiler and P. Warneck, *Chem. Phys. Lett., 54* (1978) 444.
16 F. Su, J. G. Calvert and J. H. Shaw, *J. Phys. Chem., 83* (1979) 3185.
17 F. Su, J. G. Calvert, J. H. Shaw, H. Niki, P. D. Maker, C. M. Savage and L. D. Breitenbach, *Chem. Phys. Lett., 65* (1979) 221.
18 G. K. Moortgat and P. Warneck, *J. Chem. Phys., 70* (1979) 3639.
19 B. M. Morrison, Jr., and J. Heicklen, *J. Photochem., 11* (1979) 183.
20 B. M. Morrison, Jr., and J. Heicklen, *J. Photochem., 13* (1980) 189.
21 E. K. C. Lee and R. S. Lewis, *Adv. Photochem., 12* (1980) 1.
22 B. M. Morrison, Jr., and J. Heicklen, *J. Photochem., 15* (1981) 131.
23 C. B. Moore, *Ann. Rev. Phys. Chem., 34* (1983) 525.
24 E. J. Bowen and E. L. Tietz, *J. Chem. Soc.*, (1930) 234.
25 J. Mignolet, *Bull. Soc. R. Sci. Liege, 10* (1941) 343.
26 C. A. McDowell and L. K. Sharples, *Can. J. Chem., 36* (1958) 251.
27 C. A. McDowell and L. K. Sharples, *Can. J. Chem., 36* (1958) 268.
28 J. G. Calvert and P. L. Hanst, *Can. J. Chem., 37* (1959) 1671.
29 C. A. McDowell and S. Sifoniades, *Can. J. Chem., 41* (1963) 300.
30 C. S. Parmenter and W. A. Noyes, Jr., *J. Am. Chem. Soc., 85* (1963) 416.
31 H. S. Johnston and J. Heicklen, *J. Am. Chem. Soc., 86* (1964) 4254.
32 A. S. Archer, R. B. Cundall and T. F. Palmer, *Proc. R. Soc. London, Ser. A, 334* (1973) 411.
33 J. Weaver, J. Meagher, R. Shortridge and J. Heicklen, *J. Photochem., 4* (1975) 341.
34 N. A. Clinton, R. A. Kenley and T. G. Traylor, *J. Am. Chem. Soc., 97* (1975) 3746.
35 J. Weaver, J. Meagher and J. Heicklen, *J. Photochem., 6* (1976) 111.
36 R. J. Gill and G. H. Atkinson, *Chem. Phys. Lett., 64* (1979) 426.
37 H. Meyrahn, G. K. Moortgat and P. Warneck, *J. Photochem., 17* (1981) 138.
38 R. J. Gill, W. D. Johnson and G. H. Atkinson, *Chem. Phys., 58* (1981) 29.
39 A. Horowitz and J. G. Calvert, *J. Phys. Chem., 86* (1982) 3094.
40 A. Horowitz and J. G. Calvert, *J. Phys. Chem., 86* (1982) 3105.
41 R. Simonaitis and J. Heicklen, *J. Photochem., 23* (1983) 299.
42 G. K. Moortgat, W. Seiler and P. Warneck, *J. Chem. Phys., 78* (1983) 1185.
43 F. E. Blacet and J. N. Pitts, Jr., *J. Am. Chem. Soc., 74* (1952) 3382.
44 C. A. McDowell and L. K. Sharples, *Can. J. Chem., 36* (1958) 258.
45 R. P. Borkowski and P. Ausloos, *J. Am. Chem. Soc., 84* (1962) 4044.
46 A. P. Altshuller, I. R. Cohen and T. C. Purcell, *Can. J. Chem., 44* (1966) 2973.
47 S. L. Kopczynski, A. P. Altshuller and F. D. Sutterfield, *Environ. Sci. Technol., 8* (1974) 909.
48 D. A. Hansen and E. K. C. Lee, *J. Chem. Phys., 63* (1975) 3272.
49 P. Shepson and J. Heicklen, *J. Photochem., 18* (1982) 169.
50 P. Shepson and J. Heicklen, *J. Photochem., 19* (1982) 215.
51 P. A. Leighton, L. D. Levanas, F. E. Blacet and R. D. Rowe, *J. Am. Chem. Soc., 59* (1937) 1843.

52 F. E. Blacet and J. G. Calvert, *J. Am. Chem. Soc.*, *73* (1951) 661.
53 M. V. Encina, E. A. Lissi and F. A. Olea, *J. Photochem.*, *14* (1980) 233.
54 J. Heicklen, J. Desai, A. Bahta, C. Harper and R. Simonaitis, *J. Photochem.*, in the press.
55 J. G. Calvert and J. N. Pitts, Jr., *Photochemistry*, Wiley, New York, 1966, p. 369.
56 NASA, Chemical Kinetics and Photochemical Data for Use in Stratospheric Modeling, *Jet Propulsion Laboratory Publication 83-62*, 1983, p. 136.
57 D. Wuebbles, personal communication, 1981.